Journal of Catalysis 344 (2016) 1–15

Contents lists available at ScienceDirect

Journal of Catalysis

journal homepage: www.elsevier.com/locate/jcat

Operando XAS and NAP-XPS studies of preferential CO oxidation on Co_3O_4 and CeO_2-Co_3O_4 catalysts

Liliana Lukashuk [a,1], Karin Föttinger [a,*], Elisabeth Kolar [a], Christoph Rameshan [a], Detre Teschner [b], Michael Hävecker [b], Axel Knop-Gericke [b], Nevzat Yigit [a], Hao Li [a], Eamon McDermott [a], Michael Stöger-Pollach [c], Günther Rupprechter [a]

[a] Institute of Materials Chemistry, Technische Universität Wien, Getreidemarkt 9/BC/01, 1060 Vienna, Austria
[b] Department of Inorganic Chemistry, Fritz-Haber-Institute of the Max-Planck-Society, Faradayweg 4-6, 14195 Berlin, Germany
[c] University Service Center for Transmission Electron Microscopy, Technische Universität Wien, Wiedner Hauptstraße 8, 1040 Vienna, Austria

ARTICLE INFO

Article history:
Received 5 July 2016
Revised 25 August 2016
Accepted 1 September 2016

Keywords:
Cobalt oxide
PROX
Hydrogen
Operando XAS
NAP-XPS
Ceria promoter
Oxidation state

ABSTRACT

Co_3O_4 is a promising catalyst for removing CO from H_2 streams via the preferential CO oxidation (PROX). A Mars-van-Krevelen redox mechanism is often suggested but a detailed knowledge especially of the oxidation state of the catalytically active surface under reaction conditions is typically missing. We have thus utilized operando X-ray absorption spectroscopy to examine structure and oxidation state during PROX, and near atmospheric pressure-XPS at low photoelectron kinetic energies and thus high surface sensitivity to monitor surface composition changes. The rather easy surface reduction in pure CO (starting already at ~100 °C) and the easy reoxidation by O_2 suggest that molecularly adsorbed CO reacts with lattice oxygen, which is replenished by gas phase O_2. Nevertheless, the steady state concentration of oxygen vacancies under reaction conditions is too low even for XPS detection so that both the bulk and surface of Co_3O_4 appear fully oxidized during PROX. Furthermore, the effect of adding CeO_2 (a less active material) to Co_3O_4 was studied. Promotion of Co_3O_4 with 10 wt% CeO_2 increases the reduction temperatures in CO and H_2 and enhances the PROX activity. Since CeO_2 is a less active material, this can only be explained by a higher activity of the Co-O-Ce interface.

1. Introduction

The hydrogen-fueled proton exchange membrane fuel cell (PEMFC) is an attractive pollution-free power source for portable and stationary applications, but it requires hydrogen of high purity. The current hydrogen production is mainly based on methane steam reforming, oil/naphtha reforming, and coal gasification to syngas ($CO + H_2$), followed by the water-gas shift reaction (WGSR) (i.e., $CO + H_2O \rightarrow CO_2 + H_2$), and separation processes [1–3]. However, even after these processes the hydrogen produced still contains CO traces, typically 1–100 ppm, which bind strongly to the Pt/C anode and reduce the number of Pt surface sites available for H_2 adsorption/dissociation and oxidation, thus lowering the overall efficiency of PEMFC [4]. For long-term PEMFC operation, a very deep purification of hydrogen for obtaining CO-free H_2 is thus crucial. Purification of H_2 can be achieved through Pd membrane separation, catalytic methanation (i.e., $CO + 3H_2 \rightarrow CH_4 + H_2O$) or preferential oxidation of CO (PROX) (2) [5,6].

$$\text{PROX}: \quad CO + H_2 + 0.5O_2 \rightarrow CO_2 + H_2$$
$$\Delta H_{298} = -283 \text{ kJ/mol} \qquad (1)$$

During catalytic methanation there is an apparent loss of H_2 which can be avoided for PROX, provided this reaction runs selective. However, the competitive adsorption of CO and H_2 on the catalyst surface and similar enthalpies of CO oxidation (2) and H_2 oxidation (3) facilitate their parallel occurrence:

$$CO + 0.5O_2 \rightarrow CO_2 \quad \Delta H_{298} = -283 \text{kJ/mol} \qquad (2)$$

$$H_2 + 0.5O_2 \rightarrow H_2O \quad \Delta H_{298} = -242 \text{ kJ/mol} \qquad (3)$$

The challenge of PROX is thus to achieve a high CO oxidation rate at moderate temperature and with high selectivity, thereby avoiding H_2 oxidation and methanation, accompanied by resistance toward deactivation (e.g., by coking).

The PROX catalysts most frequently investigated are supported noble metals (e.g., Pt, Rh, Ru, Ir) [3], but none of them meets all

* Corresponding author.
E-mail address: karin.foettinger@tuwien.ac.at (K. Föttinger).
[1] Current address: Johnson Matthey Technology Centre, PO Box 1, Belasis Avenue, Billingham, Cleveland, TS23 1LB, UK.

http://dx.doi.org/10.1016/j.jcat.2016.09.002
0021-9517/

requirements. In recent years, due to their price and limited availability, increasing attention has been directed toward non-noble-metal alternatives, such as transition metal oxides. Especially copper-based and cobalt-based catalysts show potential for PROX [7–15]. While copper-based PROX catalysts exhibit high activity even at low temperature, they operate in a rather narrow temperature window (50–160 °C) and show limited stability at higher temperatures [16–18].

In contrast, cobalt-based catalysts operate in a wider temperature window, offering a higher stability with regard to hot spots induced by the exothermicity of both CO oxidation and H_2 oxidation. However, the onset temperature of CO oxidation of current catalysts needs to be lowered, and the ideal catalyst should start working already at room temperature (RT) and have high activity and selectivity around 80–100 °C. Thus, research has been directed toward the improvement of the catalytic performance of cobalt oxide catalysts via addition of other reducible metal oxides (e.g., MnO_2, CeO_2) [14,15,19–21]. Nevertheless, the improvement of effective cobalt-based catalysts requires a fundamental understanding of the active catalyst.

Previous studies of PROX on cobalt-based catalysts have demonstrated that the oxidation state of cobalt is the most important factor. For example, a study of the active cobalt species using substituted cobalt spinel oxides, such as $Zn_xCo_{3-x}O_4$ ($x = 0–1$), $Al_xCo_{3-x}O_4$ ($x = 0–2.5$), and $Fe_xCo_{3-x}O_4$ ($x = 0–2.5$), has shown that octahedrally coordinated Co^{3+} surface ions are crucial for high oxidation activity and selectivity in the presence of H_2 [22]. However, another investigation of PROX over Co_3O_4 and CoO has demonstrated that CoO shows higher activity than Co_3O_4, while the metallic Co phase induces methane formation, resulting in a decrease of selectivity [11]. Thus, the current understanding of PROX over cobalt-based catalysts remains ambiguous with contradicting results concerning the role of Co^{2+} and Co^{3+}. This is due to the fact that the investigations of PROX on cobalt-based catalysts were mostly based on ex situ analyses of the catalysts. A recent in situ X-ray absorption (XAS) study of Gewade et al. on Co_3O_4-CeO_2 catalyst has revealed that the catalyst (bulk) is Co_3O_4 under the reducing PROX reaction environment at 175 °C when CO oxidation is dominant [14]. But it is still unclear whether the surface is also composed of Co_3O_4 or is partially reduced. Furthermore, the structure of ceria is unknown.

As outlined, the correlation between the cobalt (surface) oxidation state and its catalytic activity is an important topic of cobalt oxide PROX catalysis. This encompasses also fundamental questions of how Co_3O_4 undergoes reduction in (pure) H_2 or CO atmospheres and how to preserve the ideal cobalt oxide over a wide temperature range, thereby preventing reduction to metallic cobalt e.g. on hot spots, which promotes side reactions. Several studies have already been performed to obtain an understanding of Co_3O_4 reduction in H_2 that include primary structural investigations by in situ X-ray diffraction (XRD), in situ environmental electron microscopy, and temperature programmed reduction (TPR) [23–26]. In contrast to H_2 reduction, Co_3O_4 reduction in CO atmosphere has been much less investigated and very little is known on a fundamental level [27].

In this study, we aimed to improve the understanding of PROX over cobalt oxide catalysts by applying in situ (operando) methodology, in particular to shed light on the correlation of the surface and bulk oxidation state with the specific activity/selectivity [28–30]. While the Mars van Krevelen mechanism is widely accepted for CO oxidation on Co_3O_4, the oxidation state and structure of the catalyst under PROX conditions and whether (surface) reduction of Co_3O_4 by CO or reoxidation by O_2 proceeds faster is unknown. This applies particularly for the surface. Thus, we combined advanced operando methods, i.e. in situ XAS at the Co K edge to reveal bulk structural changes, whereas for surface composition changes (information depth around 0.5 nm) in situ near atmospheric pressure X-ray photoelectron spectroscopy (NAP-XPS) was applied. One should be aware, however, that due to different cell designs the different operando studies may still show differences (for details see Section 3.6). Along these lines, cobalt oxide reduction in H_2 or CO was also examined, because none of the previous studies examined, for the same material, the oxidation state in H_2, CO, and in the PROX reaction mixture. We also investigated the promotional role of CeO_2 on the improvement of Co_3O_4 reactivity.

2. Experimental

2.1. Catalyst synthesis

Co_3O_4 was used as received from Fluka (purity 99.5%). CeO_2-Co_3O_4 with 10 wt% CeO_2 loading was prepared via wet impregnation of Co_3O_4. In a typical synthesis, 0.504 mg of $Ce(NO_3)_3{\cdot}6H_2O$ was dissolved in 7 mL of distilled water, added to 1.8 g of Co_3O_4, and stirred overnight. After that, the catalyst was dried at 110 °C for 3 h and further calcined at 400 °C for 2 h.

CeO_2 powder catalyst has been prepared via surfactant-assisted precipitation method. In a typical synthesis, 6 mmol of surfactant Pluronic F-127 (Sigma-Aldrich, used as received) was dissolved in 200 mL distilled water at room temperature and 10 mmol of Ce $(NO_3)_3{\cdot}6H_2O$ was added to it. After that, an aqueous solution of NaOH (0.3 mol L^{-1}) was added to the solution under vigorous stirring until pH 10 was reached. Then the obtained mixture was aged at 90 °C for 3 h. The precipitate was filtered, washed 3 times with deionized water, and dried at 110 °C for 12 h. Afterward, the powder was calcined at 500 °C for 4 h.

Absence of impurities like sodium (in surface(near) regions) in both materials was confirmed by overview XPS spectra.

Basic characterization of the materials was done by N_2 physisorption, X-ray powder diffraction (XRD) and high resolution transmission electron microscopy (HRTEM). Experimental details are provided as supplementary material.

2.2. Temperature programmed reduction (CO-TPR, H_2-TPR)

CO-temperature programmed reduction (CO-TPR) and H_2-temperature programmed reduction (H_2-TPR) experiments on catalysts (ca. 20 mg) were performed in a continuous-flow fixed-bed quartz reactor under atmospheric pressure. Before each experiment, the catalysts were pretreated with synthetic air (50 mL min^{-1}) at 400 °C for 30 min (heating rate 10 °C min^{-1}) to remove contaminants. The samples were then cooled to 30 °C under a flow of synthetic air and purged with helium for 5–10 min.

For CO-TPR and H_2-TPR, the pretreated samples were exposed either to a mixture of 5 vol.% CO and 95 vol.% He (CO-TPR) at RT or to 5 vol.% H_2 or 50 vol.% H_2 in He (H_2-TPR). The total flow was always adjusted to 50 mL min^{-1}. Then, the system was heated to 700 °C with a heating rate of 10 °C min^{-1}. The gas stream was analyzed by an online quadrupole mass spectrometer (Prisma Plus QMG 220, Pfeiffer Vacuum) equipped with a Faraday detector.

2.3. Catalytic preferential CO oxidation

Preferential CO oxidation on Co_3O_4 and CeO_2-Co_3O_4 catalysts was performed in a continuous-flow fixed-bed quartz reactor under atmospheric pressure. The sample (ca. 20 mg), mixed with quartz powder to avoid mass and heat transfer limitations, was loaded into the reactor and pretreated with synthetic air (50 mL min^{-1}) at 400 °C for 30 min (heating rate 10 °C min^{-1}). The sample was then cooled to 30 °C under a flow of synthetic

air, before a 1 vol.% CO, 1 vol.% O_2, 50 vol.% H_2 and 48 vol.% He mixture (total flow 50 mL min^{-1}) was introduced. Then, the system was heated to 200 °C with a heating rate of 2 °C min^{-1}. The concentrations of CO and CO_2 in the outlet stream were monitored by gas chromatography using a HP-PLOT Q column and a flame-ionization detector with a methanizer.

In addition, the following temperature programmed reaction experiments were carried out in the same setup as PROX: PROX (1 vol.% CO, 1 vol.% O_2, 50 vol.% H_2), CO oxidation (1 vol.% CO, 1 vol.% O_2), hydrogen oxidation (1 vol.% O_2, 50 vol.% H_2), CO methanation (1 vol.% CO, 50 vol.% H_2), CO_2 hydrogenation (1 vol.% CO_2, 50 vol.% H_2), and water gas shift (1 vol.% CO, 3 vol.% H_2O), reactions (total flow 50 mL min^{-1}). The gas stream was analyzed by an online quadrupole mass spectrometer (Prisma Plus QMG 220, Pfeiffer Vacuum, equipped with a Faraday detector) during heating the catalyst in the reaction mixtures from RT to 350 °C with a heating rate of 2 °C min^{-1}.

2.4. Operando XAS

Operando X-ray absorption spectroscopy studies at the Co K edge (7709 eV) were carried out in transmission geometry at the I811 beamline at the MAX-lab synchrotron radiation source, Lund University, Sweden, in a reaction cell supplied by MAX-lab II [31]. The flow cell is very similar to the continuous-flow fixed-bed laboratory quartz reactor used in the laboratory for our catalytic experiments. It consists of a heatable stainless steel holder, a plate with a window mounted onto the holder, the reaction cell compartment, and another plate with a window on top. The holder provides the heating plates and a thermocouple. Al foil with a thickness of 15 μm was used as window. Co metal foil was used for energy calibration. Higher harmonics were rejected using a double crystal monochromator detuned by −50% of the maximum Bragg intensity. Typically, ca. 2.5 mg of the catalyst diluted with 10 mg of BN was loaded into the cell and pretreated in 20 vol.% O_2 in He at 400 °C for 30 min. The sample was then cooled to RT and purged with He at RT for 15 min, before the PROX reaction mixture of 1 vol.% CO, 1 vol.% O_2, 50 vol.% H_2 and 48 vol.% He was introduced. XAS spectra were recorded at RT and during subsequent heating to 350 °C. The gas stream outlet was controlled by an MKS mass spectrometer equipped with a SEM detector. In addition to PROX, CO-temperature programmed reduction (5 vol.% CO in He) followed by O_2-temperature programmed oxidation (20 vol.% O_2 in He) and H_2-temperature programmed reduction (50 vol.% H_2 in He) experiments were performed. All experiments were carried out at ambient pressure with a total flow of 50 mL min^{-1}. The duration of each Co K edge XAS scan was 5 min.

Details on data analysis are provided as supplementary material.

2.5. Operando NAP-XPS

Operando near atmospheric pressure X-ray photoelectron spectroscopy was performed at the ISISS beamline at the synchrotron radiation facility BESSY II of the Helmholtz-Zentrum Berlin, Germany. The setup consists of a reaction cell attached to a set of differentially pumped electrostatic lenses and a separately pumped analyzer (Phoibos 150 Plus, SPECS GmbH), as described elsewhere [32]. Typically, the powder sample (ca. 30 mg) was pressed into a Tantalum grid (to minimize potential charging effects) together with a K-type thermocouple, fixed to a sapphire sample holder and mounted inside the XPS reaction cell in front of the first aperture of the differentially pumped electrostatic lens system. The heating of the samples was done from the back using an infrared laser. Before the experiments, the sample was pretreated in the XPS reaction cell by oxidation (0.5 mbar O_2 at 400 °C) until all residual surface carbon and carbonates disappeared. After cooling the sample to RT, either CO (0.15 mbar), H_2 (0.4 mbar) or the CO + O_2 + H_2 PROX mixture (1/1/12 ratio at 0.5 mbar) was introduced with the partial pressure of the gasses controlled by calibrated mass flow controllers, and photoemission spectra were recorded. Then, the sample was heated to 100, 150, 200, 250 and 300 °C with a heating rate of 5 °C min^{-1}, and photoemission spectra were acquired at these temperatures. To ensure surface specificity, the Co 2p, Ce 3d, and C 1s core-level regions were recorded using selected photon energies that resulted in photoelectrons with 200 eV kinetic energy and a 0.6 nm inelastic mean free path for cobalt. The gas phase composition was monitored on-line by an electron impact Quadrupole mass spectrometer and multichannel gas chromatograph, which were connected to the XPS cell via a gas dosing valve. Details on data analysis are described in the supplementary material.

3. Results and discussion

3.1. Structural characterization of Co_3O_4 and CeO_2-Co_3O_4 catalysts

The structural and textural properties of Co_3O_4 and CeO_2-Co_3O_4 catalysts were studied by X-ray diffraction (XRD) (Fig. S1) and N_2 adsorption (Fig. S2). For Co_3O_4 the (average) crystallite size was 28 nm, for CeO_2-Co_3O_4 it was again 28 nm for Co_3O_4 but 4 nm for CeO_2, as determined from XRD. The specific surface area, average pore diameter, and pore volume for Co_3O_4 and CeO_2-Co_3O_4 were similar: 38.3 m^2/g, 14.2 nm, 0.15 cm^3/g for Co_3O_4 and 36.2 m^2/g, 13.0 nm, 0.15 cm^3/g for CeO_2-Co_3O_4. Thus, wet impregnation of Co_3O_4 with 10 wt% CeO_2 did not alter the textural properties of Co_3O_4. The structure and morphology of the catalysts were further investigated by high resolution transmission electron microscopy (HR-TEM). The low magnification TEM image of Co_3O_4 (Fig. 1a) illustrates that Co_3O_4 is present as nanospheres with sizes between 20 and 50 nm. The HRTEM image (Fig. 1b) shows lattice fringes with a 0.466 nm spacing that corresponds to (111) planes of Co_3O_4. (HR)TEM images were also taken for CeO_2-Co_3O_4 (Fig. 1c and d). The lattice fringes of 0.311 nm with slightly darker contrast correspond to CeO_2 (111), indicating CeO_2 particles with diameters of 5–10 nm supported on Co_3O_4. Elemental mapping by EELS and HAADF-STEM confirmed that the small CeO_2 particles were homogeneously distributed throughout the sample (Fig. S3).

3.2. PROX activity of Co_3O_4

To examine PROX reaction profiles, temperature programmed reaction experiments were performed over Co_3O_4 catalyst (Fig. 2a). Following the concentration of the educts (CO, O_2) and products (CO_2, H_2O, CH_4), three temperature windows were identified. On Co_3O_4, CO oxidation is the dominant reaction from 50 to 175 °C, with only negligible amounts of H_2O being produced above 100 °C (Fig. 2a). Above 175 °C the concentration of CO and H_2O increased, while that of CO_2 decreased. At 230 °C methane formation started and water production strongly increased. The H_2O peak at 260 °C is due to reduction of Co_3O_4 (see below).

To better understand the temperature-dependence of the PROX reaction profile, the corresponding individual reactions were examined as well. This holds for reactions of the educts (CO oxidation (I), H_2 oxidation (II), CO hydrogenation (III)), as well as for reactions of products with reactants (CO_2 hydrogenation (IV), H_2O + CO (water gas shift reaction) (V)).

$$2CO + O_2 \rightarrow 2CO_2 \quad (I)$$

$$2H_2 + O_2 \rightarrow 2H_2O \quad (II)$$

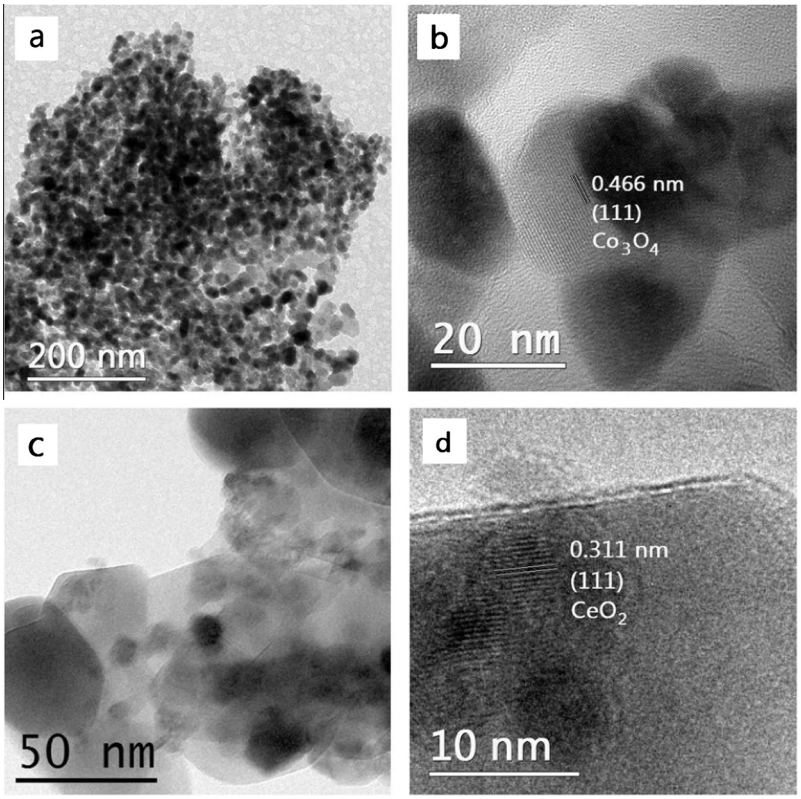

Fig. 1. (HR) TEM of Co_3O_4 (a, b), and CeO_2-Co_3O_4 (c, d).

$$CO + 3H_2 \rightarrow CH_4 + H_2O \quad (III)$$

$$CO_2 + 4H_2 \rightarrow CH_4 + 2H_2O \quad (IVa)$$

$$CO_2 + H_2 \rightarrow CO + H_2O \quad (IVb)$$

$$CO + H_2O \rightarrow CO_2 + H_2 \quad (V)$$

CO oxidation (I) starts around 75 °C and reaches a maximum at 150 °C, when 100% conversion is reached. For H_2 oxidation (II), a similar pattern is observed with the water peak at 260 °C being due to Co_3O_4 reduction (Fig. S4). For CO hydrogenation (III), methanation was observed above 225 °C with the water again peaking at 255 °C due to Co_3O_4 reduction. For CO_2 hydrogenation (IVa; Sabatier reaction), formation of CH_4 and H_2O was observed above 220 °C when the CO_2 concentration strongly decreases, whereas there was no activity for reverse water gas shift reaction (IVb; RWGS). However, the Sabatier reaction runs via CO. It might be that CO that is formed via RWGS immediately undergoes CO methanation, because CO methanation on Co_3O_4 starts in the same temperature range at around 225–230 °C (III). Note that the water peak at around 255 °C is not so pronounced because of the high concentration of water that is formed. For $CO + H_2O$ (water gas shift reaction) (V), it was observed that the conversion of CO to CO_2 starts only above 350 °C. Apparently, the presence of water hinders Co_3O_4 reduction by CO. Only a small peak of CO_2 was observed at around 250 °C.

Based on these reactivity patterns one can conclude that CO oxidation dominates up to 175 °C, between 175 and 230 °C there is both CO oxidation and H_2 oxidation occurring, and above 230 °C methane formation prevails. Secondary reactions of CO_2 with H_2 do not occur below 230 °C, and above 230 °C CO_2 and CO hydrogenation is identical (RWGS and CO methanation (II) may occur sequentially). The water gas shift does not take place below 350 °C and is thus not relevant for CO_2 formation. In order to better understand the temperature-dependent changes in selectivity we have examined the reduction behavior of Co_3O_4 in pure H_2 and pure CO. In both cases reaction with lattice oxygen creates oxygen vacancies (and water or CO_2, respectively). We will start with H_2-TPR because its behavior is somewhat simpler than that of reduction by CO. Under PROX conditions the oxygen vacancies will be replenished by gas phase oxygen but the oxidation state will depend on whether reduction or (re)oxidation dominates. Thus, the catalyst oxidation state during PROX was examined as well.

3.3. H_2-temperature programmed reduction of Co_3O_4: in situ XAS and in situ NAP-XPS

The reducibility of Co_3O_4 in H_2 was studied in a continuous-flow fixed-bed reactor with different concentrations of H_2 (5 and 50 vol. % H_2) to reveal the influence of H_2 concentration/pressure on the TPR profile (Fig. 3a). This is crucial for comparison with operando experiments (e.g., XAS and XPS), which mimic experimental conditions but cannot be carried out in exactly the same reaction environment as in a continuous-flow fixed-bed reactor. For both H_2 concentrations, two rather broad peaks were observed that can be attributed to $Co_3O_4 \rightarrow CoO$ and $CoO \rightarrow Co$ reduction (at lower and higher temperature, respectively). The absence of a larger, narrow TPR peak characteristic of the reduction of Co_3O_4 to CoO on the low-temperature side suggests that in the present case the H_2 reduction of Co_3O_4 is not a well-defined two-step reduction process consisting of two clearly separated steps (i.e., Co_3O_4 to CoO and CoO to Co, involving CoO as an thermodynamically stable intermediate). The reduction of Co_3O_4 is rather a one-step process that occurs around 290 °C. A similar effect for Co_3O_4 reduction in H_2 was observed by Kuznetsov and Kulish [33]. Based on isothermal investigations, they concluded that CoO is thermodynamically unstable below 291 °C. Therefore, Co_3O_4 undergoes reduction "di-

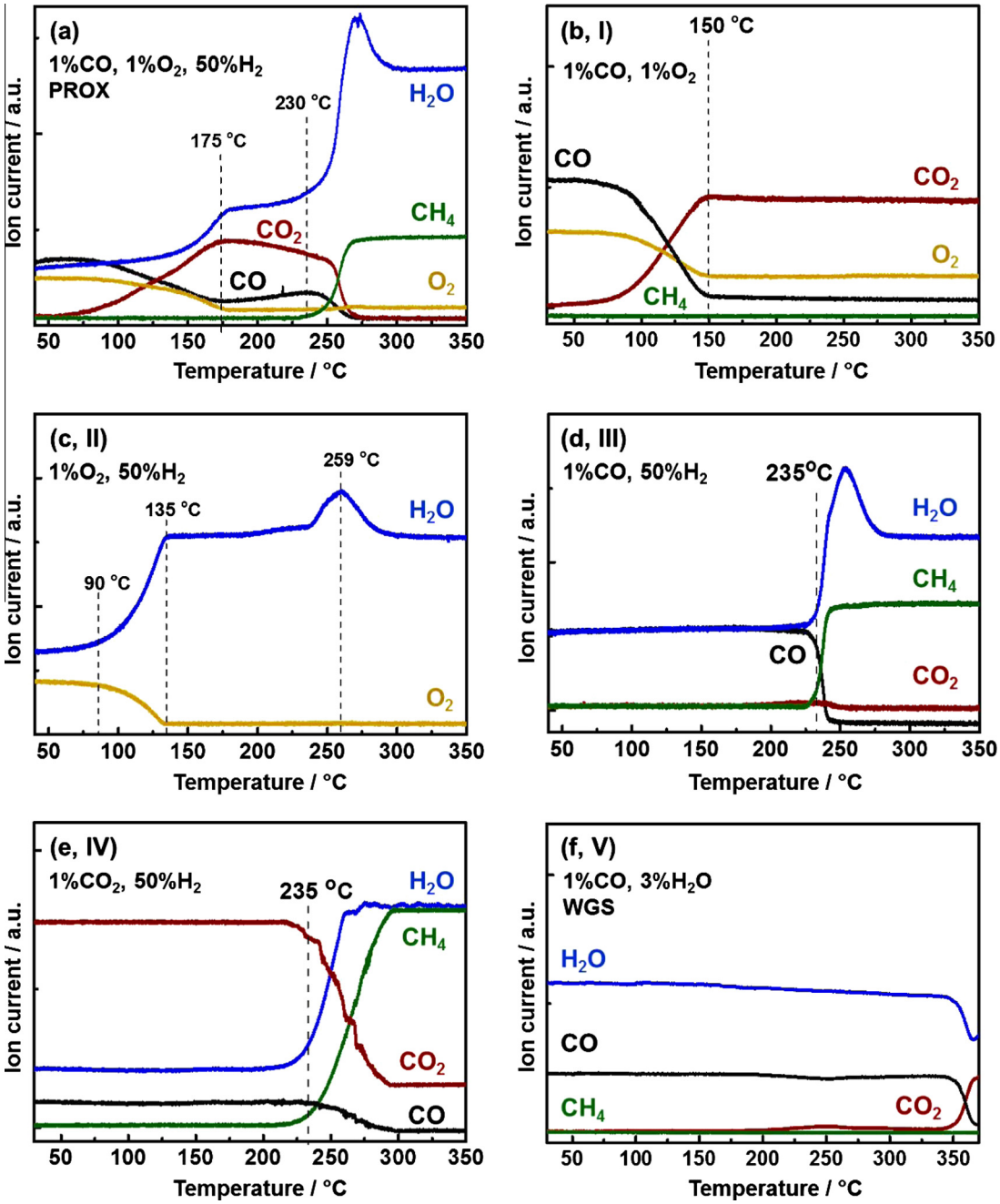

Fig. 2. Temperature programmed reactions on Co_3O_4: (a) PROX reaction (1 vol.% CO, 1 vol.% O_2, 50 vol.% H_2); (b, I) CO oxidation (1 vol.% CO, 1 vol.% O_2); (c, II) H_2 oxidation (1 vol.% O_2, 50 vol.% H_2); (d, III) CO hydrogenation (1 vol.% CO, 50 vol.% H_2); (e, IV) CO_2 hydrogenation (1 vol.% CO_2, 50 vol.% H_2); (f, V) H_2O + CO (water gas shift reaction) (1 vol.% CO, 3 vol.% H_2O), total flow 50 mL min^{-1}. I-V refer to the reaction equations given below.

rectly" to metallic cobalt. On the contrary, CoO is stable above 291 °C; thus, Co_3O_4 reduction becomes a two-step process.

The bulk electronic structure during H_2 reduction of Co_3O_4 was studied by in situ XAS while heating from RT to 400 °C in 50 vol.% H_2 in He. XANES spectra at the Co K edge, acquired during H_2-TPR of Co_3O_4 with Co foil as a reference, are shown in Fig. 3b. To quantify the extent of cobalt reduction, the H_2-TPR XANES spectra were fitted with a linear combination of reference spectra (i.e., Co_3O_4, CoO, and Co), and the result is presented in Fig. 3c. Analysis of the XANES spectra reveals that the bulk structure of Co_3O_4 remains intact up to 200 °C in H_2; at 250 °C reduction begins, and at 300 °C formation of CoO and Co (in addition to Co_3O_4) was observed. From the time-dependent in situ XANES spectra at 300 °C (Fig. S5a) it can be seen that Co_3O_4 undergoes reduction from Co_3O_4 to metallic cobalt very fast. The linear combination analysis indicates that during the first 5 min only 20% of metallic Co is present but after 15 min ~60% of cobalt atoms are metallic (Fig. S5b). At 350 °C the main phase is metallic cobalt (~90%). Based on the in situ XANES data it can be concluded that the reduction of Co_3O_4 to metallic Co proceeds via intermediate formation of CoO, but it is not a slow two-step reduction process with a well-defined CoO intermediate phase. Similar effects have been observed by Potoczna-Petru et al. and Garces et al. using TEM and in situ XRD, respectively [23,25]. The study of Potoczna-Petru et al. on Co_3O_4 particles reduction (~12 nm and 20 nm) suggests that two effects are responsible for such unusual reduction behavior: diffu-

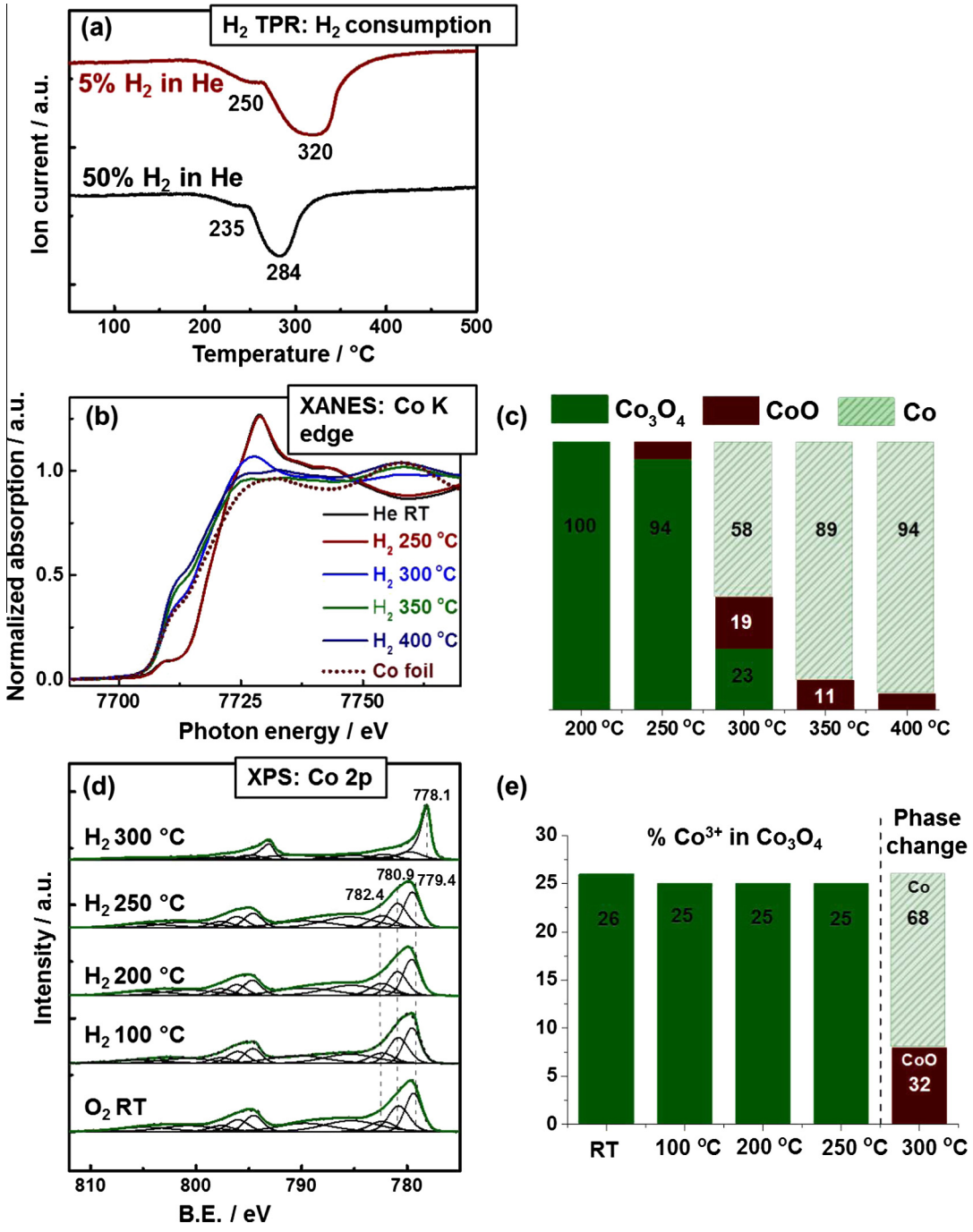

Fig. 3. (a) H_2-TPR for Co_3O_4: 50 vol.% H_2 in He (black) and 5 vol.% H_2 in He (red), total flow 50 mL min^{-1}. (b) XANES spectra at the Co K edge of Co_3O_4 during H_2-temperature-programmed reduction (50 vol.% H_2 in He, total flow 50 mL min^{-1}) and (c) amount of reduced versus oxidized cobalt calculated by linear combination of reference spectra. (d) Operando NAP-XPS H_2-temperature-programmed reduction of Co_3O_4: Co 2p region (hν = 1015 eV), 0.4 mbar H_2 and (e) amount of reduced versus oxidized cobalt calculated from linear peak fit. (For interpretation of the references to color in this figure legend, the reader is referred to the web version of this article.)

sion limitations and differences in surface defects [25]. However, a simple consecutive two-step reduction mechanism of Co_3O_4 (i.e., 1. $Co_3O_4 \rightarrow CoO$; 2. $CoO \rightarrow Co$) has been more frequently discussed in the literature [24,26]. In contrast, our in situ study rather points to the simultaneous presence of Co_3O_4, CoO, and Co under H_2 reduction conditions, in agreement with Garces and Potoczna-Petru [23,25].

According to in situ XAS, the *bulk* of Co_3O_4 remains intact up to 200 °C. Nevertheless, the *surface* of Co_3O_4 may already be partially reduced at 200 °C in H_2 and may already exhibit oxygen vacancies or defects (as indicated by the H_2 oxidation activity in Fig. 2 (II)). To address this question and to examine surface changes of Co_3O_4, NAP-XPS H_2-TPR was performed from RT to 300 °C in 0.4 mbar H_2. The Co 2p spectra are presented in Fig. 3d for a kinetic energy of 200 eV, corresponding to an inelastic mean free path of 0.6 nm (i.e., probing mainly the two topmost layers). To quantitatively elucidate the extent of Co_3O_4 reduction, the Co 2p region was fitted. The peak positions, full width at half maximum (FWHM), and constraints are presented in Table S1. According to the literature [34], the peak at 779.4 eV corresponds to Co^{3+}, the peak at 780.0 eV to Co^{2+} in CoO, and the signal at 782.4 eV to Co^{2+} in $Co(OH)_2$. For the fitting also the two shake-up satellites (surface and bulk plas-

mons) of cobalt ions were included [35], in addition to Co^{3+}, Co^{2+} in CoO and Co^{2+} in $Co(OH)_2$. In situ NAP-XPS data in the Co 2p region indicate that at temperatures up to 250 °C no significant surface reduction of Co_3O_4 to CoO took place (i.e. there was no growth of satellite peaks and the area fraction of the peak at 779.4 eV representative of Co^{3+} were 26% at RT, 25% at 100 °C, 25% at 200 °C, and 25% at 250 °C). Only above 250 °C the surface started to be reduced. At 300 °C, metallic cobalt (peak at 778.1 eV) was formed, while a small fraction of CoO was still present. The difference in the reduction temperature for Co_3O_4 in XAS and NAP-XPS experiments is likely related to the different H_2 pressures, which influence the reduction temperature of cobalt oxide, as demonstrated in Fig. 3a.

3.4. CO-temperature programmed reduction of Co_3O_4: in situ XAS and in situ NAP-XPS

During PROX, based on previously suggested mechanisms, CO is assumed to react with surface lattice oxygen and to reduce the surface. For a better understanding of the resulting oxidation state we have thus examined the interaction of Co_3O_4 with CO in a wide temperature range, performing CO-TPR in a continuous-flow fixed-bed reactor (Fig. 4a). The CO_2 profile (Fig. 4a) shows a small broader peak around 245 °C which is attributed to the reduction of Co_3O_4 to CoO. Note that the low temperature peak is much more pronounced than that in H_2-TPR (Fig. 3a). The sharp peak at 286 °C is assigned to the reduction of CoO to metallic Co, as previously reported in the literature [27]. The second peak exhibits a shoulder at higher temperature (~315 °C), which could be explained by the potential presence of intermediate wurtzite CoO beside the rocksalt CoO being reduced at somewhat shifted temperatures or by Co_3O_4 with different particles sizes. XRD, however, shows only the presence of the cubic CoO phase. Overall, the CO-TPR profile of Co_3O_4 indicates a two-step reduction with (the expected) ratio of ~1:3 between the intensities of the 1st and the 2nd peaks. Above 450 °C, small amounts of CO_2 further evolve up to 650 °C due to CO disproportionation ($2CO \rightarrow CO_2 + C$) or CO dissociation ($CO \rightarrow C + O$) on metallic Co [36–38].

Interestingly, during CO-TPR, H_2 evolution (Fig. 4b) was observed at 260 °C and 300 °C. It most likely originates from a surface reaction of CO with OH groups of the catalyst via a WGSR ($2CO + 2OH \rightarrow 2CO_2 + H_2$) [39].

The amount of CO_2 evolved from WGSR was estimated to be 10% of the total CO_2 production (i.e., most of the CO_2 is due to the cobalt oxide reduction). For CeO_2 materials WGSR is well known to be one of the mechanisms of CO_2 production [40,41]. The (nearly) parallel formation of CO_2 and H_2 suggests that the onset of reduction by CO creates active sites for the reaction of CO with surface OH groups. However, according to our reactivity data presented in Fig. 2, in the presence of gaseous H_2O WGSR only occurs above 350 °C.

To monitor changes in oxidation state during CO interaction with Co_3O_4, in situ XAS (50 mbar CO in He) and in situ NAP-XPS (0.15 mbar CO) were performed. XANES spectra at the Co K edge, acquired during CO-TPR of Co_3O_4, are presented in Fig. 4c, while linear combination fitting results displayed in Fig. 4d. As expected, the reduction profile of Co_3O_4 in CO atmosphere is different from that in H_2 atmosphere. No bulk reduction of Co_3O_4 was observed up to 200 °C; however, at 250 °C nearly 40% of CoO was present, whereas at 250 °C in H_2 the major phase was still Co_3O_4 for bulk and surface. Further heating to 300 °C in CO reduced Co_3O_4 completely to CoO, but no metallic Co was formed, and no significant time dependent reduction was observed (Fig. S6). In contrast, in H_2 atmosphere at 300 °C Co_3O_4, CoO, and Co were present. At 350 °C in CO atmosphere CoO and metallic Co were present; whereas in H_2 Co was mainly metallic. Thus, XAS suggests that the reduction of Co_3O_4 in CO atmosphere started at lower temperature and proceeded faster at 250 °C but, in contrast to reduction in H_2, it was rather a well-defined two-step reduction (with only one or two phases coexisting, but not three).

To investigate the re-oxidation of the catalyst *after* CO-TPR, O_2-temperature-programmed oxidation was performed and the results are presented in Fig. S7. From the XANES spectra it is seen that the oxidation of (metallic) cobalt starts above 200 °C, and at 300 °C the edge shifts to higher energy due to the oxidation of Co to CoO and Co_3O_4. At 400 °C, the sample was fully (re)oxidized to Co_3O_4.

It is possible that CO undergoes dissociation ($CO \rightarrow C + O$) at higher temperatures and that the carbon deposited on the surface slows down reduction. Thus, the evolution of Co 2p and C 1s upon heating from RT to 300 °C were also studied by NAP-XPS (CO 0.15 mbar) (Figs. 4 and 5). Contrary to Co_3O_4 reduction in H_2, partial reduction of Co_3O_4 started already at RT and proceeded as the temperature increased (Fig. 4e). The area fraction of the peak representative of Co^{3+} decreased from 28% (RT in O_2) to 23% at 200 °C, and an increase of the satellite peaks was observed. At 250 °C, the surface was completely reduced to CoO, as observed by the strong increase of the satellite features and shift of the peak to 780.0 eV. Thus, NAP-XPS also indicates the intermediate formation of CoO, in good agreement with operando XAS data. At 300 °C, the surface was partially reduced to metallic Co (peak at 778.1 eV), and, in addition, a small fraction of CoO was still present.

In Fig. 5a the C 1s core level region is presented, acquired during exposure of Co_3O_4 to CO from RT to 300 °C. Three carbon species were detected, at 288.2 eV, 286.1 eV, and 284.7 eV. The peak at 288.2 eV can be attributed to carbonates/carboxylates [42–44]. We assign this peak to carbonates, as observed by Jansson et al. [45] by FTIR spectroscopy. The peak at 286.1 eV may be assigned to C-O (i.e., molecularly adsorbed CO on Co^{3+} and/or Co^{2+}) or C-OH species [46,47]. In a recent study of CO adsorption on Co_3O_4 (111) thin films, Ferstl et al. reported formation of surface carbonate species (C 1s 288.5 eV) that form at defects of the film and are stable up to 127 °C, whereas molecular adsorption of CO to Co^{2+} was observed only at temperatures below −73 °C [44]. In our case, elementary carbon (C 1s binding energy at 284.7 eV) was detected in addition to carbonates and C-O, C-OH, indicating that CO dissociates on Co_3O_4 already at RT ($CO \rightarrow C + O$), depositing carbon at the surface. From the C 1s region (Fig. 5a, Table S3) it is clearly seen that the amount of elementary carbon increases at higher temperature, indicating progressive CO dissociation, while the carbonates decrease above 150 °C and the C-O species rather increase.

Based on these results, we suggest that CO adsorbs on the Co_3O_4 surface as a carbonate or molecularly, which both subsequently desorb as CO_2, extracting part of the surface lattice oxygen from Co_3O_4. The oxygen vacancies, which are formed by lattice oxygen removal, may then serve as sites for O_2 adsorption/dissociation and the neighboring Co^{x+} sites serve for CO adsorption. Also CO dissociation likely occurs on oxygen vacancies.

In any case, the two-step reduction of Co_3O_4 is more pronounced under CO than under H_2 atmosphere, in agreement with in situ XAS experiments.

Thus, XAS, NAP-XPS, and MS analysis of Co_3O_4 during CO-TPR proves three pathways: lattice oxygen removal by CO, surface water-gas shift reaction, and CO dissociation. On the contrary, interaction of H_2 with cobalt oxides proceeds via extraction of lattice oxygen from cobalt oxide only.

3.5. PROX on Co_3O_4: operando XAS and operando NAP-XPS

Based on the H_2- and CO-TPR experiments, we are now able to understand the differences in Co_3O_4 reduction in H_2 and CO atmospheres. Nevertheless, it is essential to determine the catalyst state in the PROX reaction mixture when both reducing gases (1 vol.% CO

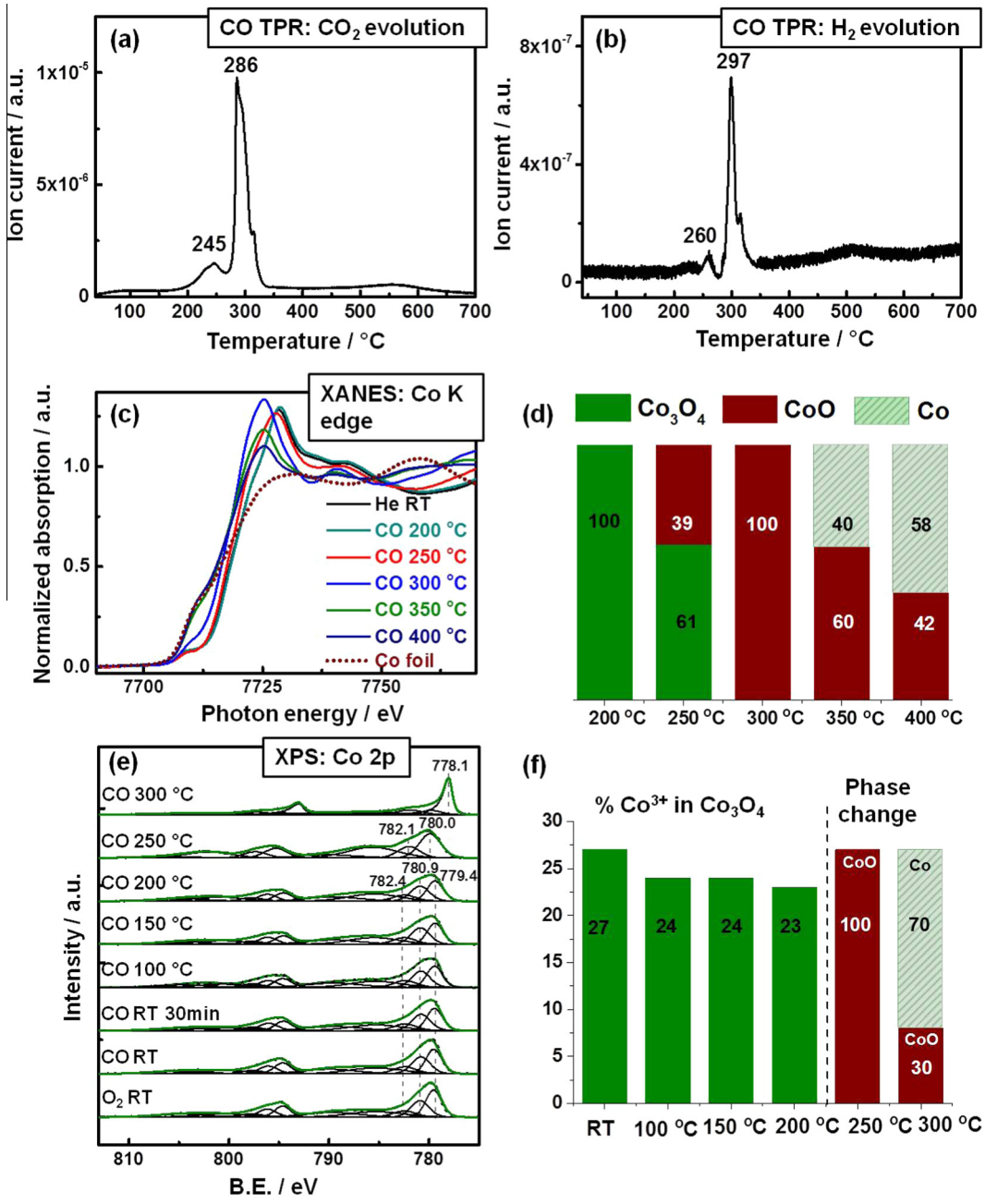

Fig. 4. (a) CO-TPR for Co_3O_4 5 vol.% CO in He, total flow 50 mL min^{-1}: CO_2 evolution and (b) H_2 evolution. (c) XANES spectra at the Co K edge of Co_3O_4 during CO-temperature-programmed reduction (5 vol.% CO in He, total flow 50 mL min^{-1}) and (d) amount of reduced versus oxidized cobalt calculated by linear combination of reference spectra. (e) Operando NAP-XPS CO-temperature-programmed reduction (0.15 mbar): Co 2p region (hν = 1015 eV); (f) amount of reduced versus oxidized cobalt calculated from linear peak fit.

and 50 vol.% H_2) are simultaneously present and, in addition, there is an oxidative (1 vol.% O_2) gas. The oxidation state of Co_3O_4 was thus studied during PROX employing (again) operando XAS, while the surface changes were studied by operando NAP-XPS. The reaction conditions and reaction environment for operando XAS were very similar to those of a continuous-flow fixed-bed reactor in the laboratory. The operando MS data are shown in Fig. 7.

The operando Co K edge XANES spectra of Co_3O_4 during heating from RT to 350 °C in the PROX reaction mixture are displayed in Fig. 6a, and linear combination fitting results are shown in Fig. 6b. The analysis of XANES reveals that from RT to 250 °C the phase of the catalyst did not change and that solely Co_3O_4 was present. As shown by the catalytic experiments in the laboratory reactor in Fig. 2a, starting around 70 °C CO oxidation took place and around 150–170 °C water production set in. Interestingly, methane production started at 230 °C and increased with temperature, even though the bulk structure of the catalyst was still Co_3O_4. However, the catalyst surface may have already exhibited defective/reduced structure (see below). Only at 300 °C Co_3O_4 was partially reduced to CoO (14%) and metallic Co (11%). At 300 °C, CO and O_2 were fully consumed via hydrogenation and the excess H_2 reduced the catalyst, as in pure H_2. Heating Co_3O_4 in the PROX reaction mixture to 350 °C induced further reduction of cobalt oxide to metallic Co (around 70%).

A comparison of operando XANES spectra during PROX with H_2-TPR and CO-TPR spectra demonstrates that the reduction of Co_3O_4

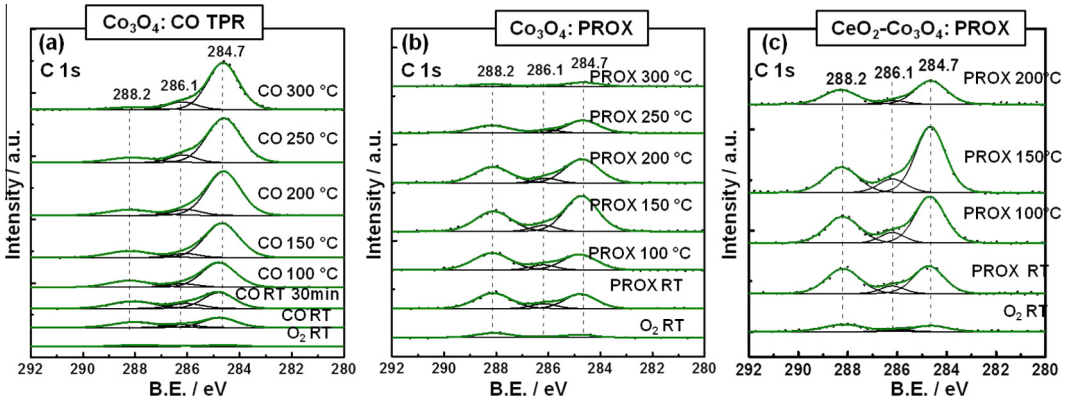

Fig. 5. C 1s region (hν = 465 eV) for operando NAP-XPS during (a) CO-TPR of Co_3O_4 (0.1 mbar CO); (b) PROX over Co_3O_4 (1.5 ml/min O_2 + 1.5 ml/min CO + 17 ml/min H_2, 0.5 mbar); (c) PROX over CeO_2-Co_3O_4 (1.5 ml/min O_2 + 1.5 ml/min CO + 17 ml/min H_2, 0.5 mbar).

in the PROX reaction mixture sets in at least 50 °C higher than those in H_2/He or CO/He atmospheres. Reduction of cobalt oxide in H_2/He started directly above 250 °C, and at 300 °C 60% of the catalyst was already metallic Co, whereas in CO/He atmosphere the reduction started at 250 °C, but at 300 °C CoO was the major single phase.

It seems apparent that the comparably lower reduction state of Co_3O_4 in the PROX reaction mixture, in comparison with H_2/He or CO/He atmospheres, is due to the reoxidation of the catalyst surface by gas phase oxygen. At lower temperature up to 170 °C, CO reaction dominates over H_2 reaction, between 170 and 230 °C H_2 reaction increases, and above 230 °C the reactants CO and H_2 rather react with each other than to reduce the catalyst. At high temperature the gas phase oxygen, together with produced water and the oxygen supplied by CO dissociation, reoxidize the surface. Clearly, above 250 °C the excess of hydrogen leads to increasing Co_3O_4 reduction, as demonstrated by the O_2-H_2 TPR (Fig. S4), since even in 1 vol.% O_2, 50 vol.% H_2 (in He) Co_3O_4 reduction starts at 260 °C.

According to operando XANES, it was evident that the (bulk) oxidation state of Co_3O_4 did not change in the selective PROX temperature window, in which CO oxidation was the dominant reaction. However, it remains to be answered whether the *surface* of Co_3O_4 was partially reduced during PROX, and if surface carbon was also present when O_2 was one of the reactants. Therefore, operando NAP-XPS was also performed during PROX. It should be mentioned that the ratio between CO, O_2 and H_2 was 1/1/12 due to the total pressure limitation (0.5 mbar) of NAP-XPS. Although the reaction conditions are somewhat different from those of a continuous-flow fixed-bed reactor and operando XAS, NAP-XPS may still help to gain further insights. The catalytic data obtained by mass spectrometry during NAP-XPS and XAS experiments are included for comparison in Fig. 7.

The evolution of Co 2p and C 1s under PROX conditions was studied from RT to 300 °C. Fig. 6c shows Co 2p spectra that clearly demonstrate the stability of the Co_3O_4 phase up to 250 °C. Even at 300 °C no Co_3O_4 reduction to CoO was detected during PROX. Thus, in contrast to H_2- and CO-TPR, for which the surface of Co_3O_4 started to reduce at lower temperature and for which a mixture of CoO and metallic Co was present at 300 °C, Co_3O_4 did not undergo surface reduction at 300 °C (even after 30 min) when O_2 was present during PROX and available for surface re-oxidation. To confirm this, CO and O_2 were switched off from the PROX reaction mixture at 300 °C and in H_2 Co_3O_4 was rapidly reduced to CoO and Co (after 5 min the surface was mainly metallic) (Fig. 6e). Thus, the presence of O_2 prevents reduction of the catalyst and its deactivation. The presence of a minor amount of reduced Co species observed at 300 °C in the corresponding operando XAS experiments, which are not found in the XPS experiments at this temperature, can be attributed to a slightly shift higher of the reduction to higher temperatures due to the different characteristics of the NAP-XPS cell.

In the C 1s region (Fig. 5b, Table S4) the formation of carbonates, C-O species and elementary carbon were detected. The presence of O_2 apparently does not fully remove elementary carbon but lowers its concentration, as compared to that observed during CO-TPR. This is true especially above 150 °C, when carbon oxidation takes place. For the CO-TPR experiment carbon increased continuously with increasing temperature. This confirms that elementary carbon originates from CO dissociation (and is clearly not an impurity). The carbonates and C-O species also decreased at higher temperature.

3.6. Correlation of oxidation state and catalytic performance in PROX

Because of differences in the design of the cells/reactors and the conditions applied (i.e., dead volumes, pressures, pellet in XPS vs sieve fraction of the catalyst used in the reactor and XAS cell, total flows, contact time between catalyst and reacting molecules), the temperature onset for the PROX reaction as well as for reduction in H_2 and CO differs for the NAP-XPS cell, the XAS cell, and the fixed-bed flow reactor in the laboratory. This particularly applies to NAP-XPS measurements, whereas conditions are much more similar for XAS and laboratory reactor experiments. Nevertheless, the trends observed for operando NAP-XPS, operando XAS and fixed bed flow reactor data are still in good agreement which allows us to correlate the oxidation state of cobalt and the catalytic performance in PROX.

Therefore, based on the operando information of the surface and bulk oxidation state of Co_3O_4 we can now try to understand its temperature-dependent selectivity. Up to 250 °C, both the surface and bulk remain fully oxidized, only above 250 °C XANES indicates partial reduction of Co_3O_4 to CoO (14%) and Co (11%). It is thus reasonable (and in agreement with previous knowledge) to conclude that this "metallization" around 250 °C switches the selectivity from PROX to CO hydrogenation to methane. NAP-XPS detected minor surface reduction at 300 °C but this offset may be due to different flow conditions (and a smaller fraction of H_2). The amount of elementary C, C-O and carbonate species is rather low at 250 °C and even lower at 300 °C.

The situation is more complex below 250 °C, for which both methods indicate a fully oxidized Co_3O_4 surface and bulk, despite the change in selectivity around 170 °C. According to the reactivity patterns in Fig. 2, the decrease in CO_2 concentration and increase in

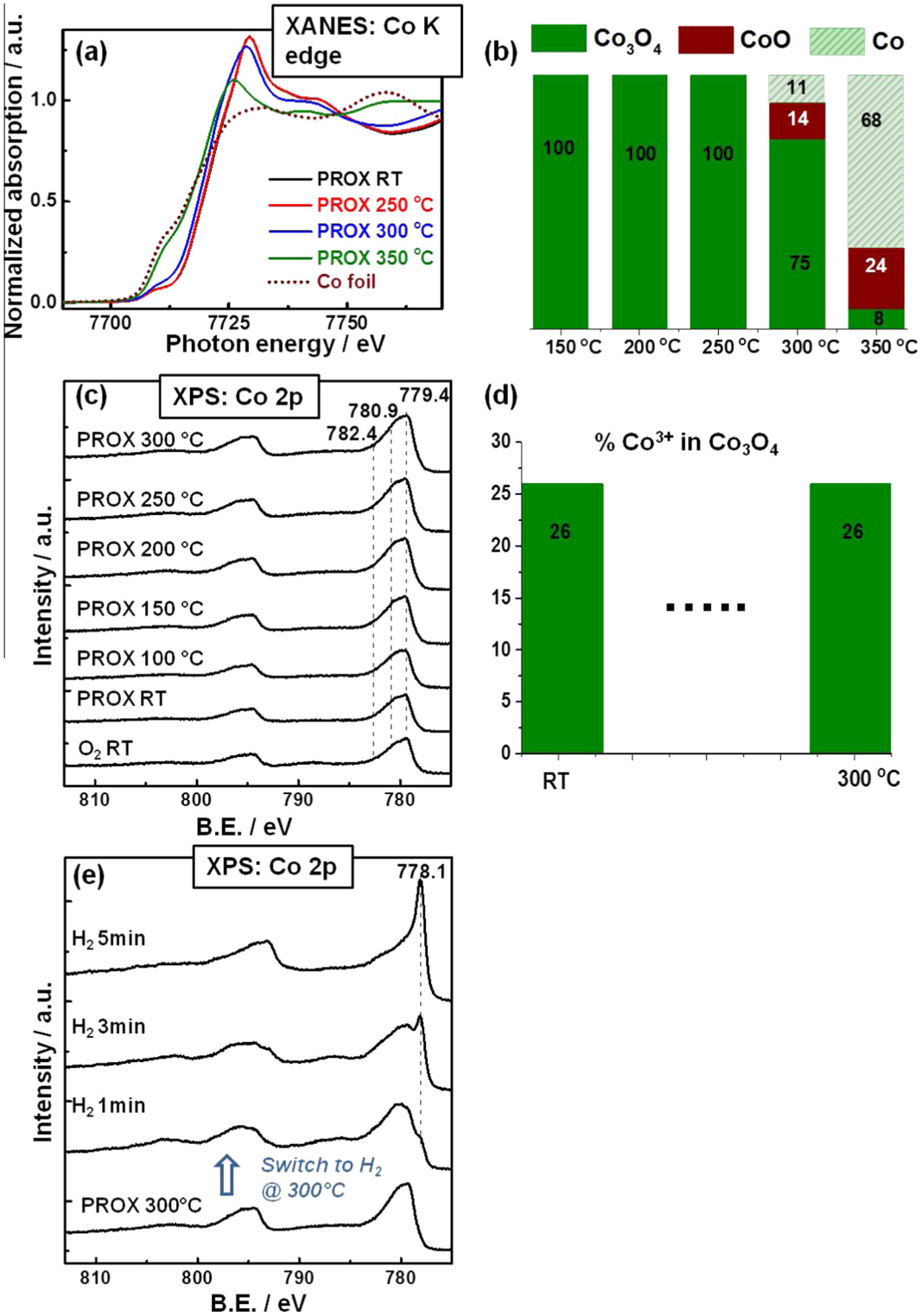

Fig. 6. (a) XANES spectra at Co K edge of Co_3O_4 PROX (1 vol.% CO, 1 vol.% O_2 50% H_2 in He, total flow 50 mL min^{-1}) and (b) amount of reduced versus oxidized cobalt calculated by linear combination of reference spectra. (c) Operando NAP-XPS during PROX over Co_3O_4 (1.5 ml/min O_2 + 1.5 ml/min CO + 17 ml/min H_2, 0.5 mbar): Co 2p region (hν = 1015 eV); (d) amount of oxidized cobalt calculated from linear peak fit; (e) operando NAP-XPS after switching the gas flow from the PROX reaction mixture to H_2 only at 300 °C over Co_3O_4, 17 ml/min H_2, 0.5 mbar: Co 2p region (hν = 1015 eV).

CO concentration starting at 175 °C is clearly due to competitive hydrogen oxidation, whereas RWGS can be excluded. A likely explanation for the increase in the competitive H_2 oxidation is that H_2 oxidation has been reported to have a larger apparent activation energy than CO oxidation (52 and 74 kJ/mol for CO oxidation and H_2 oxidation on Co_3O_4/CeO_2, respectively) [15], which explains the stronger increase of the H_2 oxidation rate with temperature as compared to the CO oxidation rate, even though the reaction onset temperature is very similar (Fig. 2 (I) and (II)). Due to the competition of H_2 and CO for the limited amount of O_2 available under PROX conditions, the low concentration of CO at high conversions, the differences in activation energies and the fact that

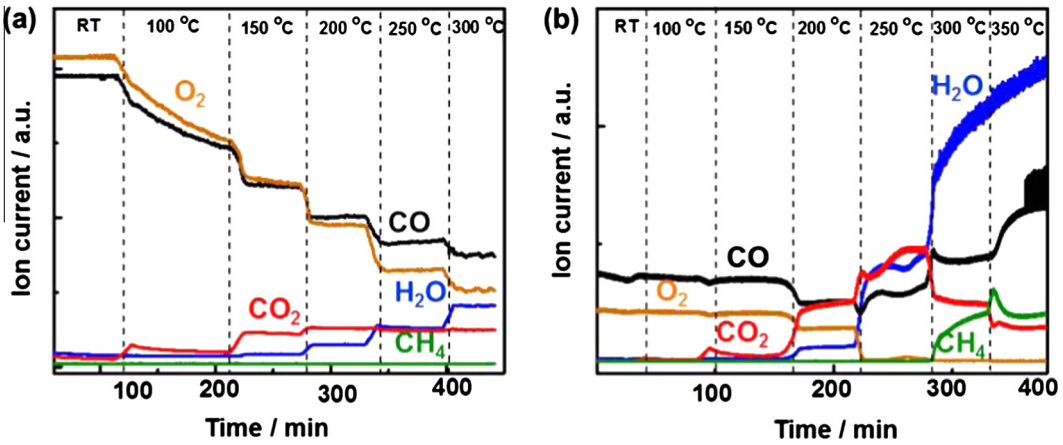

Fig. 7. MS data of PROX on Co_3O_4 recorded during (a) operando NAP-XPS; (b) operando XAS at the Co K edge.

H_2 is present in large excess, the selectivity to CO_2 decreases as H_2 oxidation speeds up.

Another potential contribution to the decreasing CO oxidation selectivity could be the onset of CO desorption between 150 and 220 °C, as indicated by the CO-TPD profile (Fig. S8), providing more available sites for H_2 oxidation (assuming site blocking by adsorbed CO which could prevent the coadsorption of hydrogen). Thus, H_2 oxidation activity would increase in the 150–220 °C temperature range, whereas CO oxidation selectivity decreases. This suggestion is also confirmed by the hydrogen oxidation temperature programmed experiment (Fig. 2(II) and S4), in which the hydrogen oxidation on Co_3O_4 catalysts started already at 90 °C and increased rapidly to 135 °C, whereas during PROX H_2 oxidation started only around 150 °C. Interestingly, (in the absence of CO) H_2 oxidation takes place already above 90 °C, despite measurable Co_3O_4 reduction in H_2 started only around 250 °C. Similar to PROX conditions, we suggest that the concentration of oxygen vacancies serving as O_2 activation sites is apparently too low to be detected by XPS and bulk-sensitive techniques like XAS.

Referring to the operando C 1s spectra, the amount of elementary C, C-O and carbonate species is increasing up to 150 °C and decreasing above 150 °C, indicating effective carbon oxidation.

With respect to the detailed reaction mechanism, the current steady-state experiments provide only limited information, however. We assume that during PROX CO adsorbs on Co_3O_4 molecularly (linearly adsorbed to cobalt cations) and also as a carbonate. Both species eventually (have) extract(ed) lattice oxygen from the Co_3O_4 surface, inducing vacancy formation. The vacancies that are formed then serve as sites for O_2 adsorption/dissociation and for reaction with another CO molecule adsorbed on the cobalt cation. However, despite this Mars-van-Krevelen mechanism the steady state concentration of oxygen vacancies is even below our NAP-XPS detection level so that the catalyst appears "fully oxidized". Furthermore, CO adsorbed on a cobalt cation might undergo dissociation, thereby depositing elementary carbon and creating oxygen that either fills an oxygen vacancy or reacts with another CO molecule (CO disproportionation). Depending on temperature, elementary carbon may be re-oxidized to CO_2.

Further details and, in particular, the contribution of the individual reaction paths can, however, not be exploited based on the current measurements. For example, we are currently unable to evaluate whether the observed carbonate species are intermediates to CO_2 formation or rather spectators. Studies involving isotopes and concentration modulation are planned for the near future.

3.7. PROX on CeO_2-Co_3O_4: operando XAS, operando NAP-XPS

Previous studies have reported that modification of Co_3O_4 with CeO_2 enhanced the activity for CO oxidation, preferential CO oxidation, hydrocarbon oxidation, and diesel soot oxidation [15,48–51]. However, the exact nature of the promotional role of CeO_2, especially in PROX, is unknown and calls for operando XAS and NAP-XPS studies. We modified Co_3O_4 by wet impregnation with an aqueous solution of $Ce(NO_3)_3$. This resulted in homogeneously distributed CeO_2 particles on Co_3O_4 (Figs. S2 and S3) and enhanced the catalytic activity for PROX (Fig. 8a). Already at 150 °C, CO oxidation reached its maximum and the temperature window for CO oxidation was widened by ~25 °C (i.e., methane production started at around 255 °C).

The promotional effect is even more clear from the reaction rates and CO conversion data during catalytic PROX between 40 and 180 °C, presented in Table 1 and Fig. 8b. The $T_{50\%}$ temperature (i.e., the temperature at which 50% CO conversion is reached) for Co_3O_4 is 139 °C, whereas for CeO_2-Co_3O_4 $T_{50\%}$ is 108 °C. The $T_{90\%}$ temperature of Co_3O_4 is 170 °C, and for CeO_2-Co_3O_4 it is 142 °C. This promotional effect (~30 °C shift) is remarkable, because the onset temperature for (pure) CeO_2 prepared as a reference catalyst is ~275 °C (Fig. S9).

TOF values were estimated assuming that Co^{3+} cations are the active sites in analogy to the work of Harutás group. Co_3O_4 nanoparticles possess mainly (111) facets as revealed with HRTEM, in agreement with Xie et al. [52] who described the morphology of the nanoparticles as truncated octahedra, surrounded by eight (111) and six (001) planes. (111) and (001) facets do not contain octahedrally coordinated Co^{3+}, only in the sub-layers. Thus, Xie et al. [1] suggested that the active sites for CO oxidation are surface defects located in the corners and edges of the spherical particles, with the Co^{3+} being exposed in these defects. They proposed a fraction of surface defects of around 5–10% of Co^{3+} for Co_3O_4 nanoparticles with a mean size of 20 nm. In alternative approach we estimated the turnover frequencies based on the total number of surface Co atoms per m^2 Co_3O_4 thus avoiding an assumption on the nature of active sites. Again we assumed a certain distribution of low index planes from the shape of the nanoparticles ((111) and (001) planes as described above) and calculated the number of surface Co atoms per m^2. In this way we obtain the lowest (theoretical) limit of TOF values (TOF^{II}) assuming all Co surface atoms are active.

Fig. 8c shows the operando Co K edge XANES spectra of the CeO_2-Co_3O_4 catalyst during PROX, upon increasing the tempera-

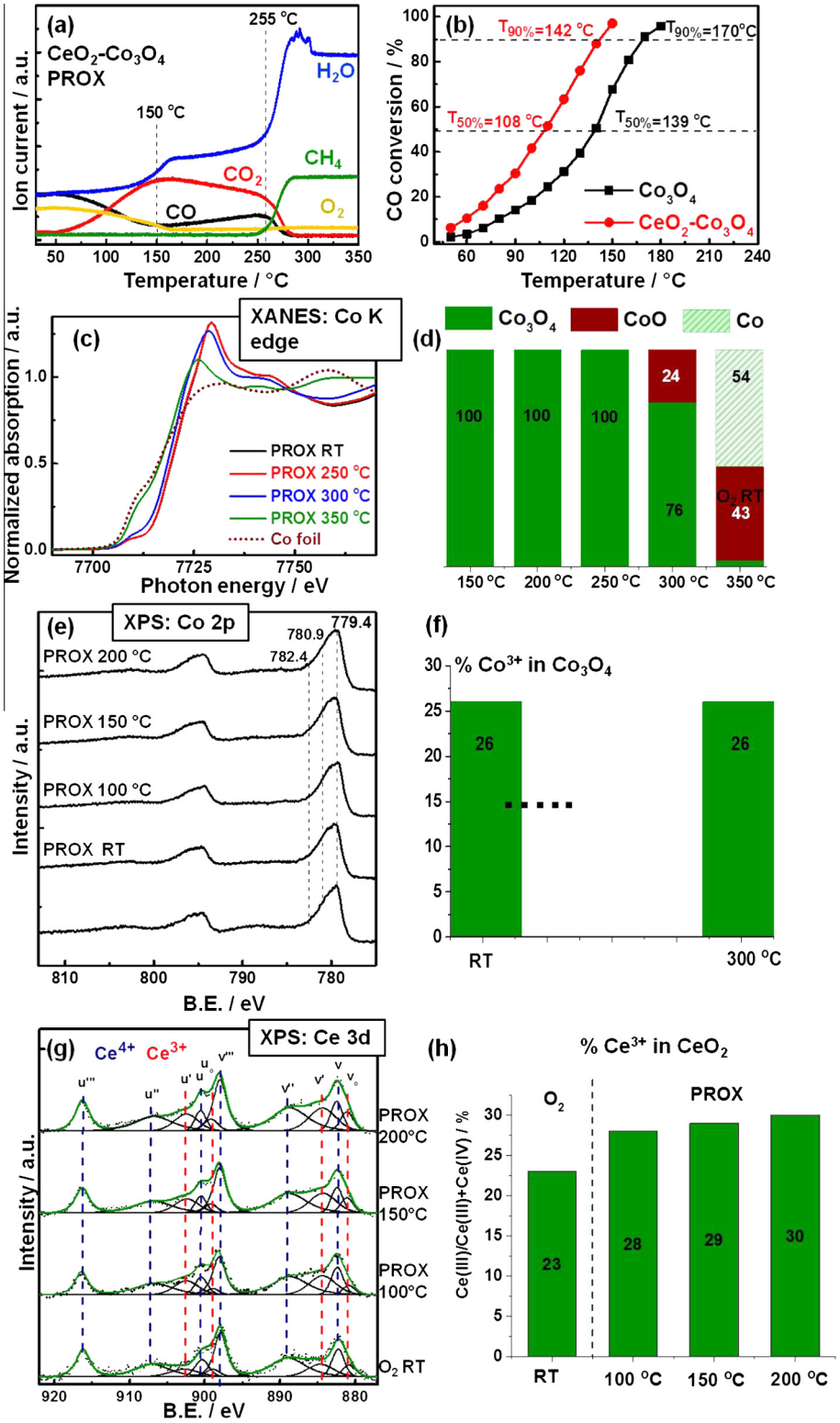

Fig. 8. (a) Temperature programmed PROX reaction on CeO_2-Co_3O_4; (b) CO conversion for Co_3O_4 and CeO_2-Co_3O_4 in the presence of 1 vol.% CO, 1 vol.% O_2, 50 vol.% H_2, total flow 50 mL min^{-1}. (c) XANES spectra at the Co K edge of CeO_2-Co_3O_4 under PROX conditions (1 vol.% CO, 1 vol.% O_2 50% H_2 in He, total flow 50 mL min^{-1}) and (d) amount of reduced versus oxidized cobalt calculated by linear combination of reference spectra. (e) Operando NAP-XPS during PROX over CeO_2-Co_3O_4 (1.5 ml/min O_2 + 1.5 ml/min CO + 17 ml/min H_2, 0.5 mbar): Co 2p region (hν = 1015 eV); (f) amount of oxidized cobalt calculated from linear peak fit; (g) Ce 3d region (hν = 1110 eV) and (h) concentration of Ce^{3+} determined by XPS.

ture from RT to 350 °C. Similar to Co_3O_4, XANES of CeO_2-Co_3O_4 reveals that up to 250 °C the Co_3O_4 oxidation state did not change. This agrees with the study of CeO_2-Co_3O_4 by Gawade et al. who reported that Co did not change its electronic structure at 175 °C in the active and selective PROX region [14]. A further increase of temperature led to the reduction of the catalyst, as evident from

Table 1
Reaction rates of CO conversion and turnover frequencies (TOF) for Co_3O_4 and CeO_2-Co_3O_4 in 1 vol.% CO, 1 vol.% O_2, 50 vol.% H_2 at a total flow of 50 mL min^{-1}.

	S_{BET}[a].(m^2/g)	$T_{10\%}$[b] (°C)	$T_{90\%}$[c] (°C)	$r_{70°C}$[d] (mol/s·g)	$R_{70°C}$[e] (mol/s·m^2)	$R_{Co3O4\_70°C}$[f] (mol/s·g)	[g]$TOF_{\_70°C}$ (s^{-1})	[h]$TOF^{ll}_{\_70°C}$ (s^{-1})
Co_3O_4	38.3	80	170	1.02×10^{-6}	2.66×10^{-8}	1.02×10^{-6}	$0.12–0.24 \times 10^{-2}$	3.3×10^{-3}
CeO_2-Co_3O_4	36.2	60	142	2.65×10^{-6}	7.32×10^{-8}	2.94×10^{-6}	$0.35–0.70 \times 10^{-2}$	9.0×10^{-3}

[a] BET surface area from N_2 sorption.
[b] Reaction temperature for 10% CO conversion.
[c] Reaction temperature for 90% CO conversion.
[d] Reaction rate of CO oxidation at 70 °C per gram of a catalyst.
[e] Normalized specific reaction rates of CO oxidation on a unit surface area at 70 °C.
[f] Reaction rates on the basis of amount of Co_3O_4 at 70°C.
[g] Turnover frequency of Co^{3+} sites at 70°C assuming 5–10% of Co^{3+} in surface defects as active sites according to [1].
[h] Alternative calculation of turnover frequency at 70°C based on all surface Co atoms (ll, lower limit).

the shift of the absorption edge to lower energy (Fig. 8c), explaining the selectivity change to methanation. When comparing operando XANES of CeO_2-Co_3O_4 and Co_3O_4, differences in the extent of cobalt oxide reduction for CeO_2-Co_3O_4 and Co_3O_4 are observed. It seems that the first is more difficult to reduce to metallic cobalt. At 300 °C, no metallic cobalt was formed in the case of CeO_2-Co_3O_4, whereas 11% of cobalt was metallic for the unpromoted catalyst.

Moreover, an increase of the reduction temperature of cobalt oxide for CeO_2-Co_3O_4 compared with Co_3O_4 catalyst was found by means of CO- (∼11 °C) and H_2-TPR (∼35 °C for 5 vol.% H_2 and 16 °C for 50 vol.% H_2) performed in a continuous-flow fixed-bed reactor (Figs. S10 and S11). All this might account for the broadening of the temperature window for CO oxidation on CeO_2-Co_3O_4.

The Co and Ce surface changes and the evolution of adsorbates during PROX were also examined by operando NAP-XPS, with Co 2p for CeO_2-Co_3O_4 presented in Fig. 8e. Again, we compare the catalytic data obtained by mass spectrometry during NAP-XPS and XAS experiments in Fig. 9. Similar to Co_3O_4, there are no significant changes of the Co 2p spectra. In the C 1s region, the formation of carbonates and elementary carbon was again detected and they also decreased above 150 °C (Fig. 5c). Interestingly, the concentration of elementary carbon with respect to carbonate and C-O, C-O-H species during PROX was higher on CeO_2-Co_3O_4 than on Co_3O_4 (Tables S5).

To monitor the Ce^{4+}/Ce^{3+} evolution, Ce 3d spectra were recorded for CeO_2-Co_3O_4 during PROX, and the representative spectra are presented in Fig. 8g. The signal of the Ce 3d level has a complex satellite structure reflecting hybridization between the Ce 4f and O 2p states. This results in two sets of spin-orbital multiplets u and v that are associated with $3d_{3/2}$ and $3d_{5/2}$ contributions, respectively [53,54]. The peaks of v, v″ and v‴ correspond to a mixing configuration of Ce(IV) ($3d^94f^2$) $O(2p^4)$, Ce(IV) ($3d^94f^1$) $O(2p^5)$ and Ce(IV) ($3d^94f^0$) $O(2p^6)$, respectively. The peaks v_o and v′ are assigned to a mixture of Ce(III) ($3d^94f^2$) $O(2p^5)$ and Ce (III) ($3d^94f^1$) $O(2p^6)$, respectively [53,54]. The same assignments are also valid for the u series of peaks. In case of our Ce 3d spectra, Ce(IV) has six peaks at binding energies of 916.5, 907.5, 900.9, 897.7, 889.3, and 882.4 eV; whereas Ce(III) peaks labeled v_o, v′, u_o, and u′ are found to appear at binding energies ranging from 880.4 to 903.9 eV, in line with the literature [53,54]. To reduce the error in the curve fitting procedure, constraints were applied. The FWHM values together with the peak positions and constraints are listed in Table S6. To estimate the (near) surface ratios of Ce(III) to the total amount of Ce species (i.e., Ce(III)/(Ce(III) + Ce(IV)) ratio), the relative areas under the fitted XPS peaks of the u_0, v_0, u′ and v'_0 with respect to the area of the entire Ce 3d region were used. It should be mentioned that reduction of Ce(IV) to Ce(III) may occur simply due to X-ray photons. Revoy et al. [55] reported reduction of the surface with monochromatic Al Kα (1486.7 eV) X-ray radiation for CeO_2. Therefore, in order to avoid beam-induced reduction, every Ce 3d spectrum was recorded from a new sample spot.

From the Ce(III)/(Ce(III) + Ce(IV)) ratios, the degree of CeO_2 reduction was determined for CeO_2-Co_3O_4 during PROX from RT to 200 °C. The Ce(III) content of the freshly oxidized sample in O_2 was 23%. Upon heating in the PROX reaction mixture (1.5 ml/min O_2 + 1.5 ml/min CO + 17 ml/min, H_2, 0.5 mbar) the Ce(IV) undergoes reduction to Ce(III), and Ce(III) concentrations are 28% at 100 °C, 29% at 150 °C, and 30% at 200 °C. Selective oxidation of CO to CO_2 starts at 50 °C and proceeds selectively up to about 125 °C. The results indicate that the relative Ce(III) concentration remains relatively constant during PROX between 100 and 200 °C.

How can the promotional effect be explained? Clearly, upon adding CeO_2 both Ce^{3+} ions and (additional) oxygen vacancies are present. However, CeO_2 by itself, with reaction onset temperatures

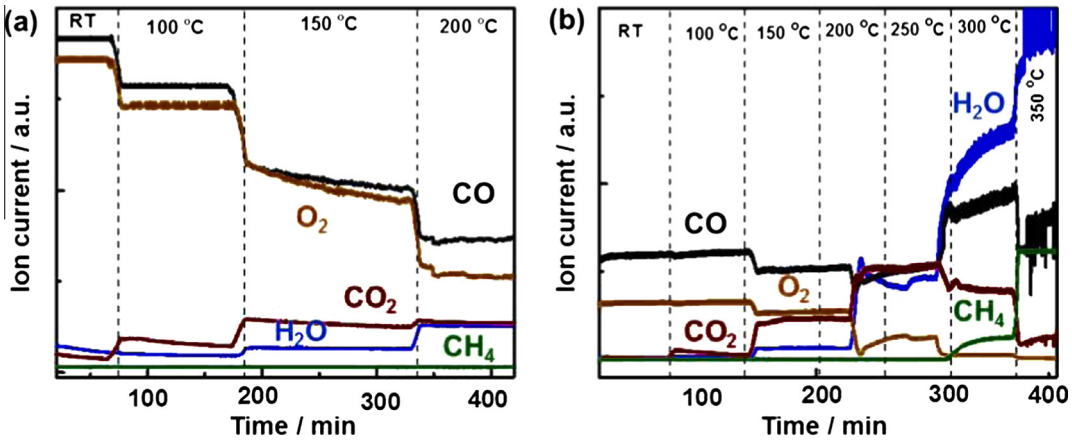

Fig. 9. MS data of PROX on CeO_2-Co_3O_4 recorded during (a) operando NAP-XPS; (b) operando XAS at the Co K edge.

around 275 °C, is much less active than Co_3O_4 (Fig. S9). We observed a similar trend in our previous study on CO oxidation [40,51]. The CeO_2 nanoparticles alone can thus not account for the enhanced activity. It is apparent that the addition of CeO_2 to Co_3O_4 must create Co-O-Co-O-Ce-O-Ce interfacial active sites that exhibit easier oxygen activation and/or oxygen vacancy formation. Moreover, incorporation of cerium (atoms) into the cobalt oxide surface (i.e., formation of local Co-O-Co-O-Ce-O-Co ensembles) and distortion of the cobalt oxide structure, forming additional vacancies, may also contribute to the catalytic improvement. The role of Ce^{3+} (e.g., for CO adsorption) remains an open question.

PROX on CeO_2-Co_3O_4 likely follows a similar reaction mechanism as on Co_3O_4, but, in addition, specific ensembles such as Co-O-Ce must play an important role, due to lower activation barriers at the interfacial sites. Further experimental and theoretical work is clearly needed to fully understand the reaction pathways of PROX on Co_3O_4 and CeO_2-Co_3O_4.

4. Conclusions

We have shown that during PROX on Co_3O_4 the catalyst appears fully oxidized (i.e., both the surface and bulk oxidation state do not change up to 250 °C). However, as revealed by reference measurements in (pure) CO, CO reduces the catalyst (surface) starting around 100 °C via reaction with lattice oxygen. However, the reoxidation by O_2 during PROX is fast enough to prevent overall reduction. Hence, despite this Mars-van-Krevelen mechanism the steady state concentration of oxygen vacancies is so low - even below our NAP-XPS detection level - that the catalyst appears "fully oxidized".

In (pure) H_2, surface and bulk reduction both start above 250 °C. While the Co_3O_4 reduction to CoO and Co around 250 °C explains the selectivity change to methanation, the change in selectivity around 170 °C from PROX (with predominantly CO oxidation) to both CO and H_2 oxidation cannot be explained by a change in (surface) oxidation state. Rather, upon increasing the temperature the difference in the increase of H_2 oxidation rate vs CO oxidation rate (higher apparent activation energy for H_2 oxidation), as well as the competition for the limited amount of O_2, is responsible for the decreasing CO oxidation selectivity. During PROX, elementary carbon, C-O species and carbonates were observed on the catalyst surface, but it is currently unclear to which extent they contribute to the overall reaction.

Adding CeO_2 to Co_3O_4 promoted the PROX activity despite that CeO_2 is much less active than Co_3O_4. This suggests that interfacial sites and/or Co-O-Ce ensembles account for the increased activity. Operando experiments did not detect differences to unpromoted Co_3O_4, apart from the presence of Ce^{3+}. The current results encourage further dynamic studies of PROX over cobalt-based catalysts in order to reveal the exact reaction pathways.

Acknowledgments

This work was supported by the Austrian Science Fund (FWF) in the framework of the Doctoral School "Building Solids for Function ("Solids4Fun") [project W1243] and by project "Cobalt Oxide Model Catalysis" ("ComCat") [I 1041-N28]. We acknowledge the Helmholtz-Zentrum Berlin for synchrotron radiation beamtime at ISISS beamline of BESSY II and the beamtime granted at the I811 beamline at the MAX-lab synchrotron radiation source, Lund University, Sweden, and support by Dr. Stefan Carlson. The research leading to these results has received funding from the European Community's Seventh Framework Programme (FP7/2007-2013) under grant agreement no. 312284. We are grateful to Dr. Klaudia Hradil and DI Werner Artner for assistance with the XRD measurements.

Appendix A. Supplementary material

Supplementary data associated with this article can be found, in the online version, at http://dx.doi.org/10.1016/j.jcat.2016.09.002.

References

[1] <http://energy.gov/eere/fuelcells/hydrogen-resources>, January 23, 2016.
[2] K. Liu, Z. Cui, T.H. Fletcher, Coal gasification, in: K. Liu, C. Song, V. Subramani (Eds.), Hydrogen and Syngas Production and Purification Technologies, John Wiley and Sons Inc., Hoboken, New Jersey, 2010, pp. 156–168.
[3] K. Liu, A. Wang, T. Zhang, ACS Catal. 2 (2012) 1165.
[4] S. Jiménez, J. Soler, R.X. Valenzuela, L. Daza, J. Power Sources 151 (2005) 69.
[5] S. Tosti, Int. J. Hydrogen Energy 35 (2010) 12650.
[6] E.D. Park, D. Lee, H.C. Lee, Catal. Today 139 (2009) 280.
[7] A. Arango-Díaz, E. Moretti, A. Talon, L. Storaro, M. Lenarda, P. Núñez, J. Marrero-Jerez, J. Jiménez-Jiménez, A. Jiménez-López, E. Rodríguez-Castellón, Appl. Catal. A 477 (2014) 54.
[8] A. Arango-Díaz, J.A. Cecilia, E. Moretti, A. Talon, P. Núñez, J. Marrero-Jerez, J. Jiménez-Jiménez, A. Jiménez-López, E. Rodríguez-Castellón, Int. J. Hydrogen Energy 39 (2014) 4102.
[9] D. Gamarra, A.L. Cámara, M. Monte, S.B. Rasmussen, L.E. Chinchilla, A.B. Hungría, G. Munuera, N. Gyorffy, Z. Schay, V.C. Corberán, J.C. Conesa, A. Martínez-Arias, Appl. Catal. B 130–131 (2013) 224.
[10] G. Marbán, I. López, T. Valdés-Solís, A.B. Fuertes, Int. J. Hydrogen Energy 33 (2008) 6687.
[11] Y. Teng, H. Sakurai, A. Ueda, T. Kobayashi, Int. J. Hydrogen Energy 24 (1999) 355.
[12] M.M. Yung, Z. Zhao, M.P. Woods, U.S. Ozkan, J. Mol. Cat. A 279 (2008) 1.
[13] Z. Zhao, M.M. Yung, U.S. Ozkan, Catal. Commun. 9 (2008) 1465.
[14] P. Gawade, B. Bayram, A.-M.C. Alexander, U.S. Ozkan, Appl. Catal. B 128 (2012) 21.
[15] M.P. Woods, P. Gawade, B. Tan, U.S. Ozkan, Appl. Catal. B 97 (2010) 28.
[16] A. Martínez-Arias, D. Gamarra, M. Fernández-García, A. Hornés, P. Bera, Z. Koppány, Z. Schay, Catal. Today 143 (2009) 211.
[17] D. Gamarra, A. Martínez-Arias, J. Catal. 263 (2009) 189.
[18] A. Martínez-Arias, A.B. Hungría, G. Munuera, D. Gamarra, Appl. Catal. B 65 (2006) 207.
[19] Q. Zhang, X. Liu, W. Fan, Y. Wang, Appl. Catal. B 102 (2011) 207.
[20] Z. Zhao, T. Bao, Y. Li, X. Min, D. Zhao, T. Muhammad, Catal. Commun. 48 (2014) 24.
[21] Z. Zhao, T. Bao, Y. Zeng, G. Wang, T. Muhammad, Catal. Commun. 32 (2013) 47.
[22] K. Omata, T. Takada, S. Kasahara, M. Yamada, Appl. Catal. A 146 (1996) 255.
[23] L.J. Garces, B. Hincapie, R. Zerger, S.L. Suib, J. Phys. Chem. C 119 (2015) 5484.
[24] H.-Y. Lin, Y.-W. Chen, Mater. Chem. Phys. 85 (2004) 171.
[25] D. Potoczna-Petru, L. Kępiński, Catal. Lett. 73 (2001) 41.
[26] M.R. Ward, E.D. Boyes, P.L. Gai, ChemCatChem 5 (2013) 2655.
[27] L. Hu, K. Sun, Q. Peng, B. Xu, Y. Li, Nano Res. 3 (2010) 363.
[28] O. Demoulin, G. Rupprechter, I. Seunier, B. Le Clef, M. Navez, P. Ruiz, J. Phys. Chem. B 109 (2005) 20454.
[29] G. Rupprechter, C. Weilach, Nano Today 2 (2007) 20.
[30] K. Föttinger, G. Rupprechter, Acc. Chem. Res. 47 (2014) 3071.
[31] S. Hannemann, M. Casapu, J.-D. Grunwaldt, P. Haider, P. Trussel, A. Baiker, E. Welter, J. Synchrotron Rad. 14 (2007) 345.
[32] A. Knop-Gericke, E. Kleimenov, M. Hävecker, R. Blume, D. Teschner, S. Zafeiratos, R. Schlögl, V.I. Bukhtiyarov, V.V. Kaichev, I.P. Prosvirin, A.I. Nizovskii, H. Bluhm, A. Barinov, P. Dudin, M. Kiskinova, Adv. Catal. 52 (2009) 213.
[33] A.N. Kuznetsov, N.F. Kulish, Izv. Akad. Nauk SSSR, Otd. Tekh. Nauk, Metall. Topl. 4 (1959) 52.
[34] M.C. Biesinger, B.P. Payne, A.P. Grosvenor, L.W.M. Lau, A.R. Gerson, R.S.C. Smart, Appl. Surf. Sci. 257 (2011) 2717.
[35] A.P. Grosvenor, S.D. Wik, R.G. Cavell, A. Mar, Inorg. Chem. 44 (2005) 8988.
[36] A.A. Khassin, T.M. Yurieva, V.I. Zaikovskii, V.N. Parmon, React. Kinet. Catal. Lett. 64 (1998) 63.
[37] Y. Chen, D. Ciuparu, S. Lim, Y. Yang, G.L. Haller, L. Pfefferle, J. Catal. 226 (2004) 351.
[38] J.E. Herrera, L. Balzano, A. Borgna, W.E. Alvarez, D.E. Resasco, J. Catal. 204 (2001) 129.
[39] K. Föttinger, R. Schlögl, G. Rupprechter, Chem. Commun. (2008) 320.
[40] J. Yang, L. Lukashuk, H. Li, K. Föttinger, G. Rupprechter, U. Schubert, Catal. Lett. 144 (2014) 403.
[41] Z. Wu, M. Li, S.H. Overbury, J. Catal. 285 (2012) 61.
[42] A.V. Shchukarev, D.V. Korolkov, Cent. Eur. J. Chem. 2 (2004) 347.
[43] Z.A. Feng, M.L. Machala, W.C. Chueh, Phys. Chem. Chem. Phys. 17 (2015) 12273.
[44] P. Ferstl, S. Mehl, M.A. Arman, M. Schuler, A. Toghan, B. Laszlo, Y. Lykhach, O. Brummel, E. Lundgren, J. Knudsen, L. Hammer, M.A. Schneider, J. Libuda, J. Phys. Chem. C 119 (2015) 16688.

[45] J. Jansson, M. Skoglundh, E. Fridell, P. Thormählen, Top. Catal. 16–17 (2001) 385.
[46] T. Ramsvik, A. Borg, M. Kildemo, S. Raaen, A. Matsuura, A.J. Jaworowski, T. Worren, M. Leandersson, Surf. Sci. 492 (2001) 152.
[47] A. Wolfbeisser, B. Klötzer, L. Mayr, R. Rameshan, D. Zemlyanov, J. Bernardi, K. Föttinger, G. Rupprechter, Catal. Sci. Technol. 5 (2015) 967.
[48] M. Dhakad, T. Mitshuhashi, S. Rayalu, P. Doggali, S. Bakardjiva, J. Subrt, D. Fino, H. Haneda, N. Labhsetwar, Catal. Today 132 (2008) 188.
[49] L.F. Liotta, G. Di Carlo, G. Pantaleo, G. Deganello, Appl. Catal. B 70 (2007) 314.
[50] C.-W. Tang, C.-B. Wang, S.-H. Chien, Catal. Lett. 131 (2009) 76.
[51] J. Yang, L. Lukashuk, J. Akbarzadeh, M. Stöger-Pollach, H. Peterlik, K. Föttinger, G. Rupprechter, U. Schubert, Chem. Eur. J. 21 (2015) 885.
[52] X. Xie, Y. Li, Z.-Q. Liu, M. Haruta, W. Shen, Nature 458 (2009) 746.
[53] E. Bêche, P. Charvin, D. Perarnau, S. Abanades, G. Flamant, Surf. Interface Anal. 40 (2008) 264.
[54] P. Burroughs, A. Hamnett, A.F. Orchard, G. Thornton, J. Chem. Soc. Dalton Trans. (1976) 1686.
[55] M.N. Revoy, R.W.J. Scott, A.P. Grosvenor, J. Phys. Chem. C 117 (2013) 10095.